Kinetics of faceting of crystals in growth, etching, and equilibrium

D. G. Vlachos, L. D. Schmidt,* and R. Aris

Department of Chemical Engineering and Materials Science, University of Minnesota, Minneapolis, Minnesota 55455

The faceting of crystals in equilibrium with the gas phase and also during crystal growth and etching conditions is studied using the Monte Carlo method. The dynamics of the transformation of unstable crystallographic orientations into hill and valley structures and the spatial patterns that develop are examined as functions of surface temperature, crystallographic orientation, and strength of interatomic potential for two transport processes: adsorption-desorption and surface diffusion. The results are compared with the continuum theory for facet formation. Thermodynamically unstable orientations break into hill and valley structures, and faceting exhibits three time regimes: disordering, facet nucleation, and coarsening of small facets to large facets. Faceting is accelerated as temperature increases, but thermal roughening can occur at high temperatures. Surface diffusion is the dominant mechanism at short times and small facets but adsorption-desorption becomes important at long times and large facets. Growth and etching promote faceting for conditions close to equilibrium but induce kinetic roughening for conditions far from equilibrium. Simultaneous irreversible growth and etching conditions with fast surface diffusion result in enhanced faceting.

I. INTRODUCTION

Faceting is the spontaneous transformation of a planar single-crystal surface into hill and valley structures[1-4] as illustrated in Fig. 1(a). It is generally believed that faceting is driven by minimization of surface free energy,[5,6]

$$\min \sum_i A_i \gamma_i \, , \tag{1}$$

where γ_i is the surface tension of the ith crystallographic orientation and A_i is its surface area. For faceting, the surface tension of some of the new crystallographic orientations must be less than that of the initial orientation to compensate for the increased surface area.

Faceting can be classified into *thermal faceting*, where the surface is altered at elevated temperatures in vacuum or an inert atmosphere, and *reaction faceting*, where the surface serves as a catalyst of a gaseous mixture (catalytic faceting) or reacts with the surrounding atmosphere to form a volatile compound (reactive etching). Thermal faceting generally proceeds much slower than catalytic faceting and is often observed only at higher temperatures. On the other hand, catalytic faceting frequently occurs with simultaneous removal of material (etching), such as in NH_3 oxidation on Pt surfaces where volatile PtO_2 is removed.[1]

Conflicting viewpoints exist in the literature as to whether surface energetics alone, Eq. (1), control the faceting process or whether growth or etching of material is the driving force for faceting.[1,7] Etching experiments have led to the conclusion that faceting might be caused by the variation of etching rate with crystallographic orientation.[1,7] The fact that catalytic faceting occurs faster and at lower temperatures than thermal faceting
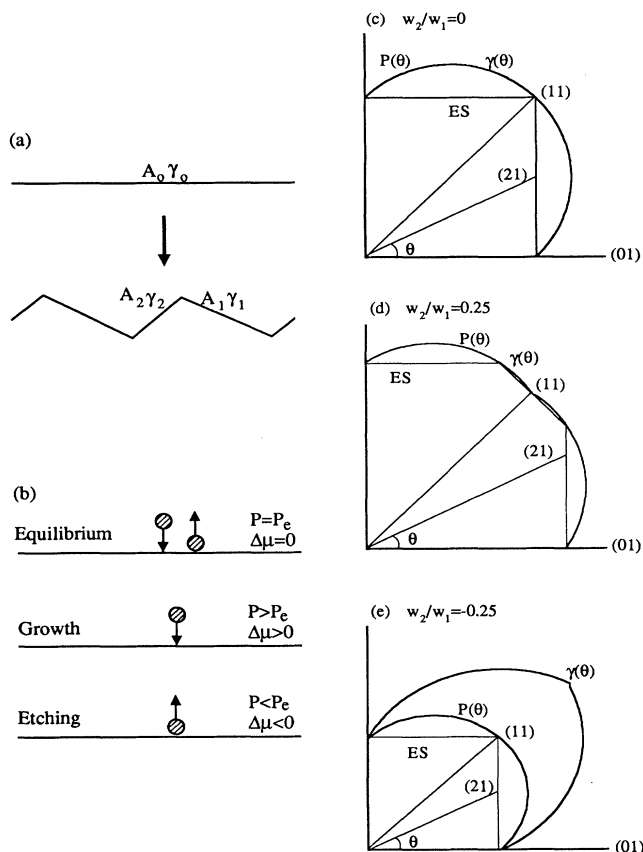

FIG. 1. Panel (a) is a schematic illustration of the faceting process. Panel (b) shows the conditions simulated. Panels (c)–(e) show γ plots, pedals P, and equilibrium shapes ES for a square lattice in two dimensions for attractive first-nearest neighbor, attractive first- and second-nearest neighbors, and attractive first- and repulsive second-nearest neighbors.

strongly suggests that *irreversible conditions promote faceting*[1] but does not answer the question whether faceting is driven by thermodynamic instability and/or irreversible conditions.

The instability of surfaces is a challenging mathematical problem because of the nonlinear dynamics involved and the rich variety of spatial patterns which develop on surfaces, as observed with optical and electron microscopies.[1] The causes which create faceting instability and how facets grow with time are intriguing questions. Faceting is also a technologically important phenomenon because it occurs in many heterogeneous systems such as in catalytic reactors during surface reaction,[1] on electrode surfaces during reaction in electrochemical cells,[8] and on semiconductor surfaces[4,9] during growth or etching.

In catalytic reactions, faceting can change the properties of adsorbed species by up to several orders of magnitude[10] because the new planes formed exhibit different surface structures from the initially flat surface. This change of properties with crystallographic orientation induced by faceting can have a profound influence on the dynamics of adsorbed overlayers and instabilities in chemical reactors. As two examples, oscillations of reaction rate in the CO oxidation on Pt (110) surfaces occur which are related to microfaceting;[11] and in microelectronics fabrication, faceting usually leads to nonplanar films of degraded quality. Thus a broad spectrum of technological applications in which faceting is involved requires a better understanding of this phenomenon in order to control instabilities in chemical reactors and to grow films of better quality.

Modeling of faceting based on capillarity concepts[12] fails to predict correctly the observed dynamics of facet formation and cannot address how complex patterns develop on surfaces. In addition, the role of nonequilibrium growth and etching conditions on faceting has not been examined. Thermal roughening (see Refs. 13 and 3) and thermal fluctuations are also not included in continuum macroscopic models, which are structurally incorrect.

The only rigorous approach to study these problems is based on molecular-level calculations. Considerable progress has been made on the understanding of the equilibrium shape (ES) of crystals, mostly by the pioneering work of Wortis and co-workers[3] using statistical mechanics and the mean-field approximation.

In this paper, the faceting of thermodynamically unstable orientations is examined at the molecular level using the Monte Carlo (MC) method to address the above issues. The organization of this paper is as follows: a brief review on ES of crystals and on the limitations of macroscopic faceting models will be given first. We then describe the transition probabilities of elementary processes and the MC method used. Surface structures and temporal behavior of faceting are then determined as functions of surface temperature and crystallographic orientation for two transport mechanisms: adsorption-desorption and surface diffusion. Faceting is examined under equilibrium, growth, and etching conditions, shown in Fig. 1(b), to elucidate the effect of irreversible conditions on faceting.

II. EQUILIBRIUM CRYSTAL SHAPE: INTERATOMIC POTENTIAL AND FACETING

The surface free energy per unit area γ_{hkl} of solids depends on the crystallographic orientation (hkl) and frequently exhibits cusps in a polar plot where the derivative of γ with respect to the angle θ from a vicinal plane is discontinuous. Cusp points are a general property of any first-order phase transition and result in flat regions in the ES of crystals.[14] The structure of solid surfaces has been analyzed using geometrical thermodynamics. The basic theorem was formulated by Wulff in 1901[5] and extended by Herring in 1951.[15] The ES of a crystal is that which minimizes the surface free energy at constant volume and is determined by the inner envelope of planes which are drawn perpendicular to and at the ends of the γ_{hkl} vectors.

Herring[15] showed that the stability of crystal surfaces with respect to faceting can be studied using the Wulff polar γ plot. This analysis leads to the important theorem that a flat surface will spontaneously facet if, and only if, its orientation is not one of those present or degeneratively present on the equilibrium form. An orientation is called degeneratively present if its Wulff plane touches but is not tangent to the equilibrium form (e.g., if the plane touches a corner or an edge of the ES). Degenerate surfaces (not included in the initial theorem by Herring) which are not present on the equilibrium form will not spontaneously facet.

A surface of a given orientation can decrease its total free energy by breaking up into other orientations if a sphere through the origin of the γ plot and tangent to the γ plot at the point corresponding to the orientation in question does not lie entirely inside the γ plot. This theorem applies equally well to inward and outward cusps. The outer envelope of such spheres is called a pedal, P_{hkl}. Mullins and Sekerka showed in 1962 that when P_{hkl} and γ_{hkl} do not coincide for an orientation (hkl), the surface free energy of this orientation can be reduced upon faceting by an amount $\gamma_{hkl} - P_{hkl}$.[16] If $\gamma_{hkl} = P_{hkl}$, this orientation is stable with respect to faceting, i.e., faceted and nonfaceted surfaces have the same free energy.

These ideas are illustrated for a square lattice in two dimensions in Figs. 1(c)–1(e). Figure 1(c) shows the γ plot when attractive first-nearest-neighbor interactions of strength w_1 $(w_1 > 0)$ are present. Only the (10) plane is present [the (100) in three dimensions] on the ES in this case, all other orientations being degeneratively present (the pedal coincides with the γ plot). When both attractive first- and second-nearest-neighbor interactions exist, the number of cusp points increases and both the (10) and (11) planes are present on the ES [the (100), (110), and (111) in three dimensions], as shown in Fig. 1(d), but unstable orientations are not present. As a consequence of the pairwise additive attractive force approximation, all orientations (hkl) of infinite extent are stable with respect to faceting.[17] When attractive first- and repulsive second-nearest-neighbor interactions $(w_2 < 0)$ are present, then all orientations become unstable but the (10) [the (100) in three dimensions], as shown in Fig. 1(e).

The solution to Eq. (1) is not unique. If the edge free energy is included in the minimization problem, the macroscopic structure should contain only one facet in order to reduce the excess amount of free energy of the edges. However, this prediction appears to be in disagreement with the quite regular distribution of facets observed experimentally.[1]

The ES of crystals is usually determined only at 0 K. To the best of our knowledge, the first exact calculations of ES at nonzero temperatures in two dimensions were done by Rottman and Wortis[18] and Avron et al.[19] Subsequently, Wortis and co-workers examined three-dimensional thermal evolution of a simple cubic lattice within the mean-field approximation[20] with first- and second-nearest-neighbor interactions. Jayaprakash and Saam[21] studied specific symmetry planes of face-centered-cubic crystal using the solid-on-solid approximation where each atom is on top of another one. Phase diagrams have been developed for first- and first- and second-nearest-neighbor interactions and the shrinking of facets with temperature has been examined.[3,20−22] Considerable effort has also been devoted to the understanding of the factors which determine the sharpness at the intersection of different surface regimes (phases) and to their relation to phase transitions.[3]

III. LIMITATIONS OF MACROSCOPIC MODELS OF FACETING

Geometrical thermodynamics provide information about the stability of surfaces. The Wulff plot is usually drawn at 0 K, and it does not address the dynamics of faceting and patterns which develop on surfaces at different temperatures. Any unstable orientation will break into other orientations given sufficient time. The time evolution of facets was described by Mullins in 1961[23] based on his thermal grooving model proposed in 1957.[24]

Three processes were examined by Mullins for mass transfer: adsorption-desorption, surface diffusion, and volume diffusion. For each individual process, the facet size L was determined as a function of time by solving the corresponding one-dimensional partial (time-dependent) differential equation. The differential equation formulated describes the transport of material caused by capillarity forces. For each elementary transport process alone, the facet size increases with time according to a power law,[23,24]

$$L \sim t^{1/n} , \qquad (2)$$

where the exponent $1/n$ and the proportionality constant depend only on the transport mechanism. $1/n$ is $\frac{1}{2}$ for adsorption-desorption, $\frac{1}{3}$ for volume diffusion, and $\frac{1}{4}$ for surface diffusion.

Experimentally, facets seem to stop growing after some time (or the rate of facet growth becomes very low) and the measured exponent $1/n$ is lower than any of the values mentioned above $(1/n \sim \frac{1}{10})$. Thus it seems that the macroscopic model does not correctly predict the dynamic evolution of faceting. In addition, Mullins's model is strictly applicable to long-time dynamics and does not treat the initial stages of facet creation and growth.

Spatial patterns observed experimentally consist of more than one facet, and patterns are in many cases quite regular, i.e., facets are almost equal in size. In the continuum faceting model of Mullins, a single facet is modeled (the dynamics of an already existing facet are analyzed), and interactions between facets are not considered. Consequently, the regularity of facet spatial distribution often observed in experiments[1] and the factors besides time which determine the density of hills and valleys are not addressed by either the Mullins model or the γ plot.

According to the continuum theory, the size of facets grown by surface diffusion or adsorption-desorption increases exponentially with temperature. There is no upper bound of temperature above which no faceting occurs. Thus *thermal roughening*[13,3] and *thermal fluctuations,* which can be of considerable importance in real materials during crystal growth and catalytic reactions, are not incorporated in this model. Thermal-roughening transitions have clearly been demonstrated by recent experiments on ^{4}He (see references in Ref. 3).

In the analysis carried out by Mullins, small deviations from low-index planes are assumed and the physical parameters are taken to be *independent* of crystallographic orientation. Improvements have been suggested in which the parameters can be orientation dependent.[25] The simultaneous role of surface diffusion and sublimation of the crystal on the dynamics have also been analyzed[26] and a theory of faceting based on orientation-dependent surface mass flow caused by electrotransport or thermotransport has been proposed.[27] However, the same concepts regarding the limitations mentioned above apply to all these modified models.

IV. RATES OF ELEMENTARY MICROSCOPIC PROCESSES AND MONTE CARLO SIMULATIONS

Based on the analysis of γ plots shown in Fig. 1, attractive first-nearest-neighbor interactions (energy $w_1 > 0$) and repulsive second-nearest-neighbor interactions (energy $w_2 < 0$) in a three-dimensional simple cubic lattice are chosen. In this prototype model all orientations are thermodynamically unstable [except the (100) plane and its equivalent planes], and metastable orientations do not exist. Hence, the dynamics of unstable surfaces and the corresponding spatial patterns which develop upon faceting can be studied. This situation is analogous to spinodal decomposition[28] where the initially unstable orientation (phase) breaks into new orientations (phases).

First- and second-nearest-neighbor interactions are probably a fair representation of the attraction (between electrons and metal ions) and the repulsion (between cations) in metals where many-body effects can also be of considerable importance. The range of interactions in metals is not very long, as predicted by the embedded atom method,[29] and thus first- and second-nearest-neighbor interactions can be a reasonable approximation. Furthermore, γ_{hkl} computed with long-range potentials is remarkably similar to that obtained by a lattice-gas model where only first- and second-nearest-neighbor in-

teractions are included.[30] Thus, by using this prototype model system, we attempt here to understand the qualitative behavior of the faceting process rather than explain in detail the change in structure of any particular material.

In this section, the transition probabilities p_a, p_d, and p_m for adsorption, desorption, and migration, respectively, are developed and the MC simulations are then described.

Adsorption from the gas phase is assumed to occur randomly on surface sites (mass transfer resistance in the gas phase is neglected). Based on kinetic theory, the adsorption probability p_a per unit time is[31]

$$p_a = k_a P ,\qquad (3)$$

where P is the gas pressure and k_a is the adsorption rate constant given by

$$k_a = \frac{s_0}{\sqrt{2\pi m k T}} .\qquad (4)$$

Here, k is the Boltzmann constant, T is the absolute temperature, s_0 is the sticking coefficient, which is assumed to be independent of surface sites, and m is the mass of an atom.

Desorption of atoms depends on the local environment of each atom. The desorption probability per unit time of an atom with n_1 first- and n_2 second-nearest neighbors is

$$p_d(n_1,n_2) = v_0 \exp(-E_d/kT)$$
$$= v_0 \exp[-(n_1 w_1 + n_2 w_2)/kT] ,\qquad (5)$$

where v_0 is the preexponential factor and $E_d = (n_1 w_1 + n_2 w_2)$ is the activation energy for desorption, which is site dependent.

For an ideal gas in contact with a solid the difference in chemical potential $\Delta\mu$ between the two phases is[32]

$$\Delta\mu = kT \ln(P/P_e) ,\qquad (6)$$

where P_e is the equilibrium crystal vapor pressure. From Eqs. (3) and (6), p_a becomes

$$p_a = k_a P_e \exp(\Delta\mu/kT) = p_{a,e} \exp(\Delta\mu/kT) ,\qquad (7)$$

where $p_{a,e} \equiv k_a P_e$.

Equilibrium prevails when the adsorption rate equals the average desorption rate. The two rates are equal at "kink" sites with exactly half the neighbors present.[33] Then $p_d(3,6) = p_{a,e}$, i.e.,

$$p_{a,e} = v_0 \exp[-(3w_1 + 6w_2)/kT] .\qquad (8)$$

Combining Eqs. (5) and (8), the desorption probability per unit time can be written as

$$p_d(n_1,n_2) = p_{a,e} \exp\{[(3-n_1)w_1 + (6-n_2)w_2]/kT\} .\qquad (9)$$

Migration is usually modeled either by the Metropolis walk[34] or Kawasaki dynamics.[35] We have used both algorithms. However, these algorithms do not actually give dynamic information because they only consider the energy difference between the initial and final states and not an activation barrier. Thus we also use the method of Gilmer and Bennema.[36] Atoms are allowed to jump to nearest-neighbor positions only. The transition probability for migration (surface diffusion) p_m is calculated based on removal from one site and creation on an adjacent site[36,37] according to

$$p_m(n_1,n_2) = p_d(n_1,n_2)(x_s/a_0)^2 ,\qquad (10)$$

where x_s/a_0 is the average distance traveled by an atom on the surface before it desorbs,[38]

$$x_s/a_0 = \exp[-(E_m - E_d)/2kT] .\qquad (11)$$

Here, a_0 is the lattice constant and E_m and E_d are macroscopic (phenomenological) activation energies for migration and desorption. Usually $E_m < E_d$,[38] and thus Eq. (10) indicates that the local energy barrier for diffusion is lower than that of desorption, Eq. (9), by $\Delta E \equiv E_d - E_m$.

We found that the qualitative behavior regarding pattern formation and dynamics is independent of the diffusion transition probability. Thus results using only the transition probability given by Eq. (10) will be presented in the following sections. Since details of the activation barrier for migration are not known, in what follows the mean diffusion distance x_s/a_0 is treated as a free parameter, as has been done previously.[36]

A major problem in simulations at low temperatures is the large difference between the maximum and minimum probabilities. As an example, at $kT/w_1 = 0.1$, the ratio of possible highest to lowest probabilities for desorption is 7×10^{20}. Use of a conventional sampling algorithm results in large rejection of test configurations (very slow sampling of phase space). As an example we found, using the Metropolis walk, that the fraction of successful attempts is $p_{\text{success}} = 0.05$ at $kT/w_1 = 0.25$ and $p_{\text{success}} = 10^{-4}$ at $kT/w_1 = 0.167$ for 10^6 MC steps.

To overcome this difficulty, we have used an extension of the n-fold method proposed by Bortz et al.[39] for first- and second-nearest-neighbor interactions in the canonical and the grand canonical ensembles. According to this method each trial is successful, and the time is updated by a continuous amount determined from the average lifetime of the surface configuration. In this algorithm we account for the a priori probability of different events before rather than after choosing a site on the surface. Efficient simulations are achieved by classifying the atoms in classes of the same transition probability. For randomly adsorbed atoms the probability for adsorption p_a at each site is the same. However, for desorption the atoms experience different local environment based on their number of first- and second-nearest neighbors. Let $N(n_1,n_2)$ be the number of atoms having n_1 first- and n_2 second-nearest neighbors; these atoms belong to the same class. In this way we define 45 possible classes for desorption and similarly for migration. The probability per unit time of choosing an event from a particular desorption class is $[N(n_1,n_2)][p_d(n_1,n_2)]$. The total probability per unit time is then

$$p^{tot}=p_{a,e} \sum_{surface} (\exp(\Delta\mu/kT)$$

$$+ \exp\{[(3-n_1)w_1+(6-n_2)w_2]/kT\}$$

$$\times[(x_s/a_0)^2+1]) . \tag{12}$$

After selecting a class, a site belonging to this class is randomly chosen and the event executed. The time is then incremented by[37]

$$\Delta t = - \ln(\xi)/p^{tot} , \tag{13}$$

where ξ is a random number $(0<\xi<1)$. The dimensionless time t^* is defined as

$$t^*=tp_{a,e} . \tag{14}$$

To speed up the algorithm, a list of atoms in each class and their coordinations is saved in the memory so that each time a successful event occurs at a site, the local environment of that site changes; the number of atoms in the affected lists and their coordinations are also changed, as well as the probabilities for choosing a class.

We have tested the above algorithm in growth on the (100) surface when only first-nearest-neighbor interactions exist. The calculated growth rates are in good agreement with the results of Gilmer and Bennema[36] where a conventional sampling method was used.

Surfaces with orientations at many points on the stereographic triangle have been simulated. However, since surfaces along the [010] zone exhibit instability in only one direction (x direction), straight facets develop at low temperatures along the y direction [see inset of Fig. 2(a)]. Thus analysis of data is simplified in one dimension and direct comparison with the one-dimensional model of Mullins[23,24] can be achieved. Hence, we present here only results from $(hk0)$ orientations. Simulations have been performed in three dimensions using the solid-on-solid approximation.[21,40] However, three-dimensional calculations without the solid-on-solid approximation were also carried out and will briefly be discussed in Sec. V A.

Simulations were usually performed on 20×120 rectangular lattices. Larger lattices up to 20×640 sites have also been used to examine the influence of the simulation box on the statistics. Periodic boundary conditions and step periodic boundary conditions[40] were applied along the unstable x direction (long dimension) and stable y direction (short dimension) of the lattice, respectively. In this way the average crystallographic orientation of the simulated surface is preserved. The use of rectangular surfaces having a longer size in the x direction provided better statistics for the distribution of facet size. In all simulations performed the size of the simulation array was quite larger than the average facet size observed.

Simulations were performed in the grand canonical ensemble (system open to mass transfer), where adsorption and desorption of atoms (with and without surface diffusion) were modeled under equilibrium ($\Delta\mu=0$) and irreversible ($\Delta\mu\neq0$) conditions and in the canonical ensemble (system closed to mass transfer) where surface diffusion was the only transport mechanism studied

($\Delta\mu=0$). Individual runs consisted typically of 10^7–(3×10^9) successful events which require 20 min to 100 h CPU time, respectively, on the Cray X-MP/464 supercomputer. Time-dependent curves shown in all following figures are the averages over 20 runs.

V. FACETING OF CRYSTALS IN EQUILIBRIUM WITH THE GAS PHASE

In this section the results of the MC calculations are presented for crystals in equilibrium with the gas phase ($\Delta\mu=0$). Results obtained for adsorption-desorption alone will be presented first and the role of surface diffusion on faceting will be discussed next. The influence of surface temperature, crystallographic orientation, and interatomic potential on surface morphology is then examined.

A. Faceting by adsorption-desorption alone

Figure 2(a) shows the initial (210) surface at $t=0$ and snapshots of the surface heated at $kT/w_1=0.25$ after $t^*=10^3$ and $t^*=8.5\times10^4$. Note that surface snapshots in all figures are arbitrarily translated from each other. The initial (210) orientation, which is not present on the ES of the crystal, breaks into a hill and valley structure. Microfacets of orientations equivalent to (100) (segments of the equilibrium orientation) develop. At low temperatures, the facets are straight along the y direction [see the inset of Fig. 2(a)] because they are (100) surfaces which belong to the ES. Upon breaking of an unstable orienta-
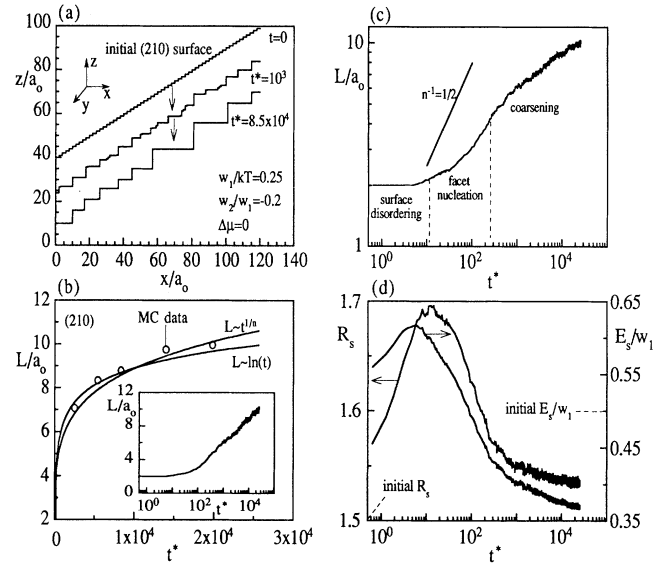

FIG. 2. Faceting of the (210) surface. Panel (a) shows two-dimensional snapshots of the three-dimensional surface for times indicated. The facets are straight along the y direction (perpendicular to the page) and thus only two-dimensional representations are shown. Panel (b) shows MC data for the average facet size L/a_0 vs time along with power and semilogarithmic law fits. The inset is a semilogarithmic plot of L/a_0 vs t^*. Panel (c) shows a logarithmic plot of L/a_0 vs t. Panel (d) shows the surface energy and roughness as functions of time.

tion a distribution of microfacets is formed (not just a single facet) in agreement with experimental observations.[1]

The average size of facets, L/a_0 (a_0 is the lattice constant) along the x axis can be calculated from a snapshot, as displayed in Fig. 2(a). At each position x, the surface is scanned along the y direction and the average height $z(x)$ per y site is calculated. If the difference of $z(x)$ from the immediately lower integer number is less than 0.5, then the terrace at the x position is considered to have some adsorbed atoms and the elevation at x is taken equal to the lower integer number. If, on the other hand, the difference is larger than 0.5, then the terrace at x is considered to have some vacancies and the elevation at x is taken as the lower integer number plus 1. Once this procedure is completed for all x, the difference in elevation between successive rows of atoms is calculated. If two rows of atoms at x and $x + a_0$ have the same elevation (they belong to the same terrace), the facet size is increased by a_0 and the procedure is repeated. Otherwise, a new terrace starts at $x + a_0$, whose size is determined. Note that the height of facets (z direction) is not an independent dimension because the crystallographic orientation of the initial surface is preserved upon faceting.

If the above procedure is repeated during the simulation, the average facet size can be determined as a function of time, as shown in Fig. 2(b) for a typical set of parameters. Figure 2(c), which shows a plot of $\log_{10}(L/a_0)$ vs $\log_{10}(t^*)$, reveals that faceting is not described by a single curve with a constant growth exponent $1/n$. The value of $1/n$ determined by fit of a power law to the data of the entire run is 0.18, as compared to $\frac{1}{2}$ predicted by the macroscopic model for adsorption-desorption.[23,24] These simulations indicate that a power law does not properly describe the dynamics of faceting and by forcing it there is not a universal value of $1/n$ as predicted by the macroscopic faceting model. The exponent $1/n$ depends on surface temperature, crystallographic orientation, interatomic potential, degree of irreversibility, and the operating mechanism, i.e., adsorption-desorption or surface diffusion (see below). A logarithmic dependence of facet size on time, i.e., $L \sim \log_{10}(t)$ does not fit the data very well either, as shown in the inset of Fig. 2(b). An increase of the simulation size did not result in an increase of the faceting exponent.[41]

We also analyze the temporal evolution of surfaces upon faceting by calculating the surface energy E_s and the roughness R_s, as shown in Fig. 2(d). E_s measures the energy loss per projected (100) site caused by formation of the surface, as compared to bulk cubic crystal, i.e., the energy of the broken first- and second-nearest neighbors. R_s is defined as the number of broken first-nearest-neighbor bonds per projected (100) site. As examples, $R_s = 1.0$ for the (100) surface and 1.5 for the (210) surface at 0 K.

Three time regimes can be distinguished in the faceting of an initially perfect surface. In the first regime, *disordering* occurs by the movement of atoms which try to reduce the number of repulsive second-nearest neighbors. In this regime, the surface energy and roughness *increase* above the initial value of the perfect surface, as shown in Fig. 2(d).

In the second regime, faceting starts and the average facet size increases quite rapidly with time whereas the surface energy and roughness drop rapidly. This regime is characterized by *nucleation of microfacets*. Nucleation starts at different times and positions, so there is lack of spatial organization, which results in quite regular but not periodic patterns. The lack of perfect periodicity of facets is associated with a configurational entropy which reduces the free energy of the system. The development of only one facet is consistent with thermodynamics at 0 K where the entropic contribution to the free energy is zero, but at high temperatures *entropy* plays a vital role in pattern formation.

In the third regime the facets continue growing but with a slower rate which seems to decrease as time proceeds. The surface energy and roughness decrease very slowly towards equilibrium. Once the surface has broken into hill and valley structures, coarsening of microfacets into macrofacets occurs, where larger facets grow at the expense of small ones. The thermodynamic driving force for further atom transport is only the very small energy required to form the edges and corners where the facets join. As faceting proceeds, fewer corners and edges exist and the driving force diminishes. As the distance between facets increases, transfer of material over longer distances is necessary so growth becomes slower. Thermal fluctuations perturb the spatial pattern and drive further faceting.

The formation of facets can be thought of as caused by attractive interactions between steps. As time proceeds the distance between steps increases and the attractive force between steps is reduced. Consequently, the driving force for faceting is lowered, and the rate of faceting decreases.

The behavior found here is analogous to the initial disordering followed by smoothing of Pt-Rh gauzes for HCN formation, as observed with scanning tunneling microscopy.[42] The temporal behavior in faceting is in agreement with surface area (measured by H_2 adsorption) versus time data during faceting of Pt gauzes in oxidation experiments.[43] These data showed that the area increases with time with an exponent $1/n$ which is smaller than any of the values predicted by the macroscopic model. Furthermore, the value of $1/n$ depended on the layer of the gauze (the deeper the layer was the lower $1/n$, i.e., faceting proceeded slower).

We have investigated the validity of the solid-on-solid approximation by also performing three-dimensional calculations where overhangs and vacancies are now allowed in the model. The qualitative behavior of the faceting transformation remains the same with that of the solid-on-solid model concerning the dynamics and regularity of surface patterns. However, some differences were observed in the exact values of the number of defects on surfaces, surface energy, and roughness. When overhangs and vacancies are allowed, the roughness and surface energy are slightly higher than the values predicted by the solid-on-solid model, and bulk vacancies have been observed in some cases. As an example, we found that the values of R_s and E_s in the solid-on-solid model are $\sim 5\%$ and $\sim 10\%$ lower than the three-dimensional

(without the solid-on-solid approximation) values at $t^* = 600$ with $kT/w_1 = 0.25$ and $w_2/w_1 = -0.2$.

B. Faceting by surface diffusion

In the preceding section, adsorption-desorption (grand canonical ensemble) was assumed to be the only means of material transport for growth of facets. In this section, surface diffusion of crystal atoms is modeled in the canonical ensemble (alone) and in the grand canonical ensemble (with adsorption-desorption). The transition probability for migration is described by Eq. (10).

Figure 3 shows the dynamics of faceting for surface diffusion alone, adsorption-desorption alone, and also with simultaneous adsorption-desorption and surface diffusion. This allows the importance of each transport mechanism to be elucidated. The qualitative behavior upon faceting is similar for the three cases with respect to dynamics and pattern formation.

However, some differences on the dynamics of faceting for the two mechanisms are noticeable. The facets formed after the same time and the exponent $1/n$ obtained by fit of a power law to the data are smaller for surface diffusion alone ($x_s/a_0 = 1$) as compared to adsorption-desorption alone. When desorption of atoms from a site occurs, redeposition can take place through the gas phase at any site on the crystal. On the other hand, surface diffusion is restricted to adjacent site jumps, i.e., material is transferred at shorter distances and thus faceting proceeds slower when surface diffusion operates if $x_s/a_0 = 1$.

However, if the activation energy for surface diffusion is smaller than that of desorption, as is believed to be generally true,[38] then x_s/a_0 can be much larger than unity. It turns out that the time for faceting by surface diffusion alone is obtained by that shown in Fig. 3 divided by $(x_s/a_0)^2$, i.e., faceting caused by surface diffusion will occur much faster than by adsorption-desorption mechanism. When $x_s/a_0 \gg 1$, surface diffusion is the dominant transport mechanism for faceting at short times.

The above observations are confirmed from simulations for the simultaneous operation of adsorption-desorption and surface diffusion shown in Fig. 3. As the surface diffusion increases faceting occurs faster at short times (small facets) but adsorption-desorption becomes dominant at long times (large facets) where material must be moved over long distances. Since the qualitative behavior is similar for both transport mechanisms, results in Secs. V C–V E will be presented only for adsorption-desorption.

C. Effect of temperature

Surface profiles obtained at different temperatures after the same dimensionless time $t^* = 10^3$ are shown in Fig. 4(a). Faceting is observed at elevated temperatures, but, as the temperature increases the number of defects increases, as shown in the inset of Fig. 4(a), and at sufficiently high temperatures the surface becomes thermally rough. Thus, at high temperatures thermal roughening prevails, and faceting is not observed.
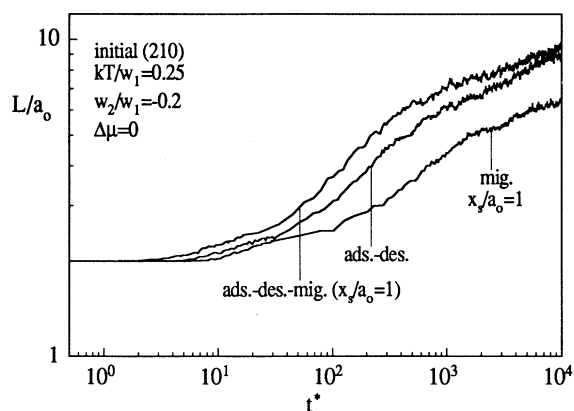
FIG. 3. Facet size vs time for adsorption-desorption alone, migration alone, and simultaneous adsorption-desorption–migration. Diffusion dominates at short times (small facets) and adsorption-desorption at long times (large facets).
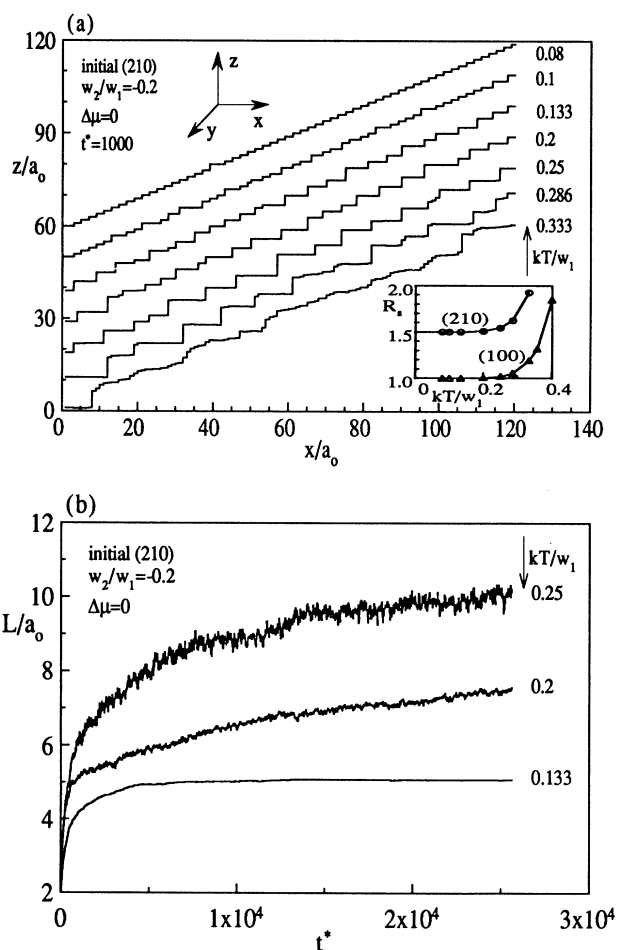
FIG. 4. Effect of surface temperature on faceting. Panel (a) shows snapshots at $t^* = 1000$ at temperatures indicated and panel (b) shows the facet size vs time for different temperatures. At low temperatures nucleation of microfacets occurs but coarsening does not.

The roughness R_s of the (010) plane versus surface temperature is shown in the inset of Fig. 4(a) for $w_2/w_1 = -0.2$. The (010) plane is thermodynamically stable for this model and thermal roughening takes place at higher temperatures than those of other planes. As the strength of second-nearest-neighbor interactions decreases, the (010) plane becomes more resistant in roughening. For $w_2/w_1 = -0.1$, roughening occurs at $w_1/kT \sim 0.5$, which is slightly lower than that of face-centered-cubic crystals found by Jayaprakash and Saam.[21]

As the surface temperature decreases, diffusion or adsorption-desorption (activated processes) become slower and facets grow slower. At low temperatures faceting is controlled by mass transfer limitations. When the temperature is sufficiently low, faceting is not observed in our simulations, as shown by the topmost profile in Fig. 4(a). Note that this profile corresponds to much longer real time than the profiles where faceting is observed. Assuming $\nu_0 = 10^{13}$ s^{-1}, the bottom and top profiles correspond to 2.2×10^{-8} and 0.6 s, respectively. That is, faceting proceeds extremely slowly at low temperatures to be observed in simulations or even in real experiments.

Figure 4(b) shows the facet size versus time for adsorption-desorption at different temperatures. Change of temperature results in variation of the growth exponent $1/n$. If the power law is forced to fit the data we find $1/n = 0.18$ at $kT/w_1 = 0.25$, $1/n = 0.15$ at $kT/w_1 = 0.20$, and $1/n = 0.13$ at $kT/w_1 = 0.133$, that is, as the temperature decreases the growth exponent drops. At high temperatures, where transport processes are fast, faceting occurs rapidly and the exponent is large. The drop of $1/n$ when temperature decreases might be due to the fact that at low T the fit is over longer real time (the fits do not correspond to the same t).

The absence of large thermal fluctuations at low temperatures prohibit coarsening of microfacets into macrofacets, as shown in Fig. 4(b). This is why thermal faceting is observed at relatively high temperatures and after long heating times as compared to catalytic faceting. Observation on vicinal Si (111) surfaces showed microfacets of certain size which did not grow with time.[9] Analogous behavior is indicated in Fig. 4(b), where at sufficiently low temperature nucleation of microfacets occurs but the small thermal fluctuations do not lead to further faceting.

D. Effect of orientation on faceting

Pt single-sphere surfaces examined with scanning electron microscopy after reaction showed that, at orientations close to the (100) poles, the Pt surfaces remain smooth and faceting is not observed.[1] Provided sufficient time, unstable orientations will facet into hill and valley structures, reducing the system free energy. Those orientations which have a larger faceting rate will vanish first, whereas those with a lower faceting rate will facet later. If the difference in times scales for faceting is sufficiently large, some areas can be faceted, whereas other areas can appear to be smooth. Here, we examine the dependence of faceting rate on crystallographic orientation.

Figure 5(a) shows the facet size versus time for several crystallographic orientations and Fig. 5(b) shows $1/n$ versus misorientation from the (100) plane. Faceting proceeds fast for the (110) orientation and very slowly for orientations close to the (100) surface. For orientations very close to the (100) surface such as the (40,1,0), no faceting is observed, although thermodynamically these orientations are unstable. We found that faceting can still be observed with adsorption-desorption but not with surface diffusion alone for small misorientations from the (100) plane. Furthermore, the smaller the misorientation is, the higher the surface temperature below which no faceting is observed.

The above observations imply that mass transfer limitations over long distances become important for small misorientations from low-index planes. For small misorientations from the (100) plane, the steps are widely separated and transport from one ledge to its neighbors through the terrace can therefore require long times. As the difference $\gamma_{hkl} - P_{hkl}$ decreases, the energy gained by faceting decreases and the faceting rate also drops. Orientations for which the difference $\gamma_{hkl} - P_{hkl}$ is small ("less unstable") would stay smooth for a very long time, whereas orientations for which the difference $\gamma_{hkl} - P_{hkl}$ is large ("more unstable") will facet fast. Note that the values of growth exponent $1/n$ predicted by the macroscopic faceting model are valid for very small misorientations from low-index planes, where the MC calculations indicate that the growth exponents are much smaller than $\frac{1}{2}$ or $\frac{1}{4}$, i.e., the agreement between the two models becomes worse for small misorientations.
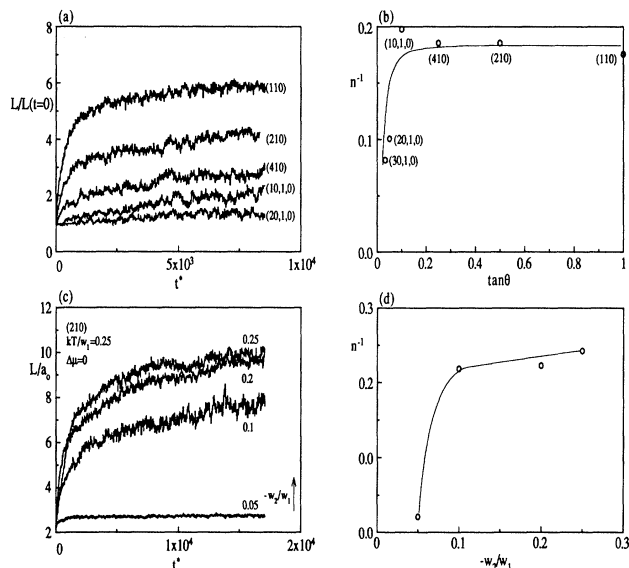

FIG. 5. Panel (a) shows the facet size vs time for different orientations and panel (b) shows $1/n$ vs misorientation from the (100) surface. Small misorientations facet very slowly. Panel (c) shows the facet size vs time for values of $-w_2/w_1$ indicated and panel (d) shows $1/n$ vs $-w_2/w_1$. Repulsive second-nearest-neighbor interactions are essential for faceting.

E. Role of second-nearest-neighbor interactions

If only first-nearest-neighbor interactions are considered ($w_1 > 0$, $w_2 = 0$), no faceting occurs for any orientation, as indicated in the γ plot shown in Fig. 1(c). The existence of repulsive second-nearest-neighbor interactions ($w_2 < 0$) is important for faceting to occur if only first- and second-nearest neighbors are assumed. Then all orientations are unstable except the (100) and no metastability exists.

The effect of strength of second-nearest neighbors on the faceting kinetics is illustrated in Figs. 5(c) and 5(d). The temporal evolution of faceting depends on the ratio $-w_2/w_1$, especially for very weak second-nearest-neighbor interactions. Faceting proceeds fast for strong repulsive interactions but very slowly at small values of $-w_2/w_1$. The dependence of stability and faceting rate on $-w_2/w_1$ indicates that the interaction potential function is an important factor in predicting the dynamics of faceting. Even if pairwise additive interactions are assumed of short range (up to second-nearest neighbors), different materials would have different interaction energies and therefore faceting would also be material dependent.

VI. FACETING WITH GROWTH

If $\Delta\mu > 0$ in Eq. (7), the adsorption flux is larger than the desorption flux, and the crystal grows from gas-phase deposition. Growth of crystals has been studied using mostly the solid-on-solid approximation on simple cubic crystals with first-nearest-neighbor interactions.[36,40] Recent calculations showed that if the supersaturation is large, crystals become rough (kinetic roughening).[44] Kinetic roughening is frequently observed in growth of organic crystals,[45] but it has received less attention than thermal roughening. The effect of growth on crystal shape and morphological instabilities such as dendritic growth have recently been examined by MC simulations.[46] However, the influence of growth on faceting transformation has not been studied and is considered next.

Surface structures under growth conditions for several values of $\Delta\mu$ in the absence of surface diffusion are shown in Fig. 6(a). At low supersaturation larger facets are formed on the surface compared to equilibrium conditions. During growth a large perturbation takes place at the interface. Thermal desorption removes atoms from all unfavorable sites, resulting in energetically favorable structures, i.e., faceted surfaces. Thus growth promotes faceting close to equilibrium.

As the supersaturation rises, defects are formed on the surface, as shown in Fig. 7(a). In growth from the gas phase, atoms stick at random positions on the crystal and the roughness increases. At high supersaturations (high growth rates) desorption is very slow in rearranging atoms compared to deposition. Above a critical supersaturation surfaces become rough rather than faceted and this phenomenon is called *growth-induced roughening* or *kinetic roughening*.

The behavior shown in Fig. 6(a) is in agreement with the results of Nozieres and Gallet,[47] who used a renormalization approach to examine the roughening transition. For a specified temperature, there is an applied force on the crystal, which here corresponds to a driving force $\Delta\mu \neq 0$, above which the facet disappears. The roughening transition is blurred under an applied force and faceting appears at a lower temperature than the thermal roughening temperature T_R of the facet. Above this temperature the facet appears rough, as indicated in Fig. 6(a).

Figure 8(a) shows the effect of faceting on the growth rate. Close to equilibrium conditions where faceting occurs, the growth rate decreases with time as facets become larger. This is due to an increase of step separation, i.e., the number of favorable sites of high coordination number is reduced as time evolves. This behavior becomes less pronounced as the supersaturation rises because the surface becomes kinetically rough and the incorporation probability increases.

A. Effect of temperature

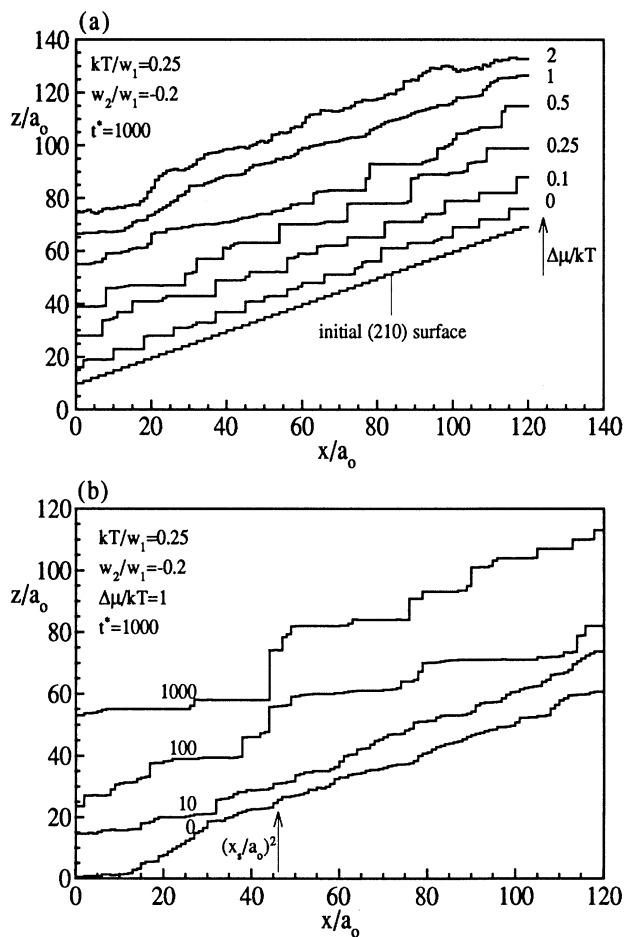We have examined the growth rate as a function of supersaturation and of surface temperature[41] and have

FIG. 6. Panel (a) shows the effect of supersaturation on surface morphology in the absence of migration. Panel (b) shows the effect of migration on surface structure under conditions where kinetic roughening would be expected.

determined the critical supersaturation versus surface temperature. Our simulations indicate that at higher temperatures the crystal becomes rough at lower supersaturation, i.e., the critical supersaturation decreases with temperature.

We have also examined surface structures at sufficiently low temperatures where mass transport limitations become important. Under equilibrium conditions no faceting was observed at low temperatures (e.g., at $kT/w_1 = 0.067$). However, we have found that under growth conditions ($\Delta\mu > 0$) facets are observed if the supersaturation is not sufficiently large. Therefore, under growth conditions energetically unstable interfaces can facet at much lower temperatures or in shorter time than under equilibrium conditions because large perturbations (fluctuations) are introduced by adsorption of atoms.

B. Effect of orientation

We have determined the growth rate versus supersaturation as the orientation of surface changes from the

(100) pole to the (110) pole of the crystallographic triangle (along the [010] zone).[41] The simulations indicate that the critical supersaturation increases from the (110) surface to the (100) surface. Orientations close to the (110) surface become kinetically rough at lower supersaturation whereas orientations close to the (100) stable pole remain smooth up to high supersaturations.

The growth rate of the stable (100) surface is lower than for any of the step surfaces, and a higher critical supersaturation is required for kinetic roughening. Hence, under the same growth conditions, the (100) surface will be more resistant in kinetic roughening than all other orientations. Consequently, the simulations indicate that thermodynamically more stable surfaces are also more resistant under nonequilibrium conditions to kinetic roughening and could be smooth planes at low temperatures whereas other surfaces would become either faceted or kinetically rough.

C. Effect of surface diffusion on kinetic roughening and faceting

In catalytic etching, it is believed that surface diffusion can be promoted by chemical reaction.[7] Therefore in many cases surface diffusion can be considered as a free
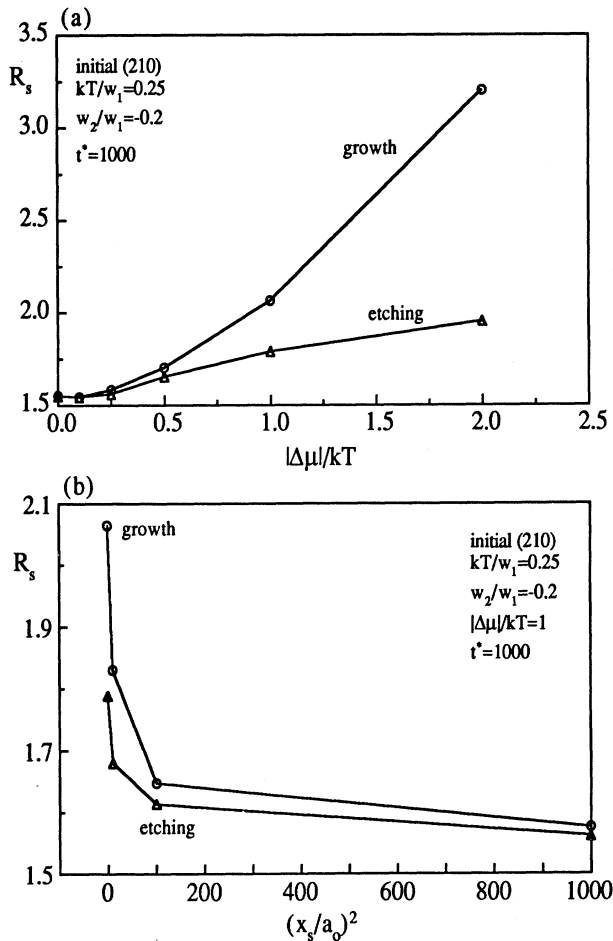

FIG. 7. Panel (a) shows the surface roughness vs supersaturation (undersaturation) in crystal growth and etching. Panel (b) shows the effect of migration on surface roughness in crystal growth and etching. At the same conditions, interfaces are rougher in growth than in etching.
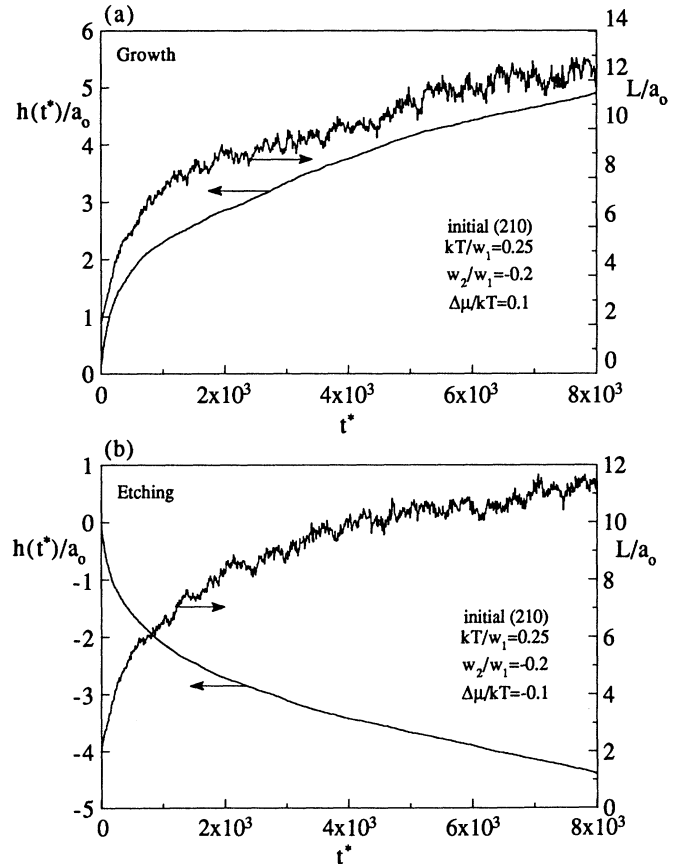

FIG. 8. Panels (a) and (b) show the number of deposited and etched layers as functions of time. Faceting reduces the growth and etching rate of surfaces.

parameter affected by the conditions of the experiment. We found that, as surface diffusion increases, atoms have sufficient time to move on the surface to favorable sites where the chance for removal back to gas phase is reduced. The number of single atoms on terraces and the surface roughness are reduced as shown in Fig. 7(b), and thus the desorption mechanism slows down, resulting in an enhanced growth rate.[41]

The role of surface diffusion on surface morphology is shown in Fig. 6(b). We have chosen conditions ($\Delta\mu/kT = 1$) where no faceting occurs in the absence of surface diffusion, as shown in Fig. 6(a), and we have allowed atoms to migrate. For sufficiently large values of surface diffusion the surface becomes faceted. A transition from kinetically rough interfaces to faceted interfaces is found as surface diffusion increases. Surface diffusion establishes local equilibrium at the interface, and atoms have sufficient time to reach favorable sites before adsorption or desorption take place. Consequently, faceting can be observed at conditions far from equilibrium (high supersaturation) if surface diffusion is sufficiently fast. Surface diffusion increases the value of
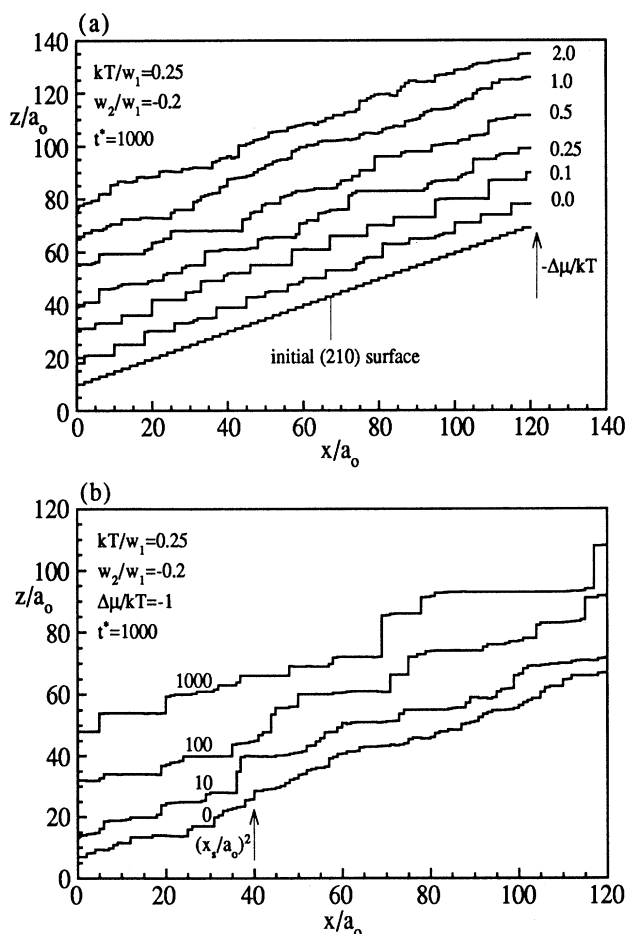

FIG. 9. Panel (a) shows the effect of undersaturation on surface morphology in the absence of migration. Panel (b) shows the effect of migration on surface structure under conditions where kinetic roughening would be expected.

critical supersaturation above which kinetic roughening of crystals occurs.

VII. FACETING WITH ETCHING

In this situation $\Delta\mu < 0$ and the gas phase is undersaturated with respect to the crystal. The surface morphology of the (210) surface under etching conditions is shown in Fig. 9(a) for various values of $-\Delta\mu/kT$ in the absence of surface diffusion. At conditions close to equilibrium, surface structures indicate that faceting is promoted, i.e., larger facets develop under etching rather than under equilibrium conditions in the same time. However, if the gas partial pressure is sufficiently small (far for equilibrium), etching occurs rapidly, and the interface becomes microscopically rough.

Calculation of etching rate versus undersaturation at different surface temperatures indicates that as the temperature increases the etching rate is enhanced because desorption of atoms is an activated process.[41] Decreasing the gas pressure results in higher etching rates. An asymptotic maximum etching rate is obtained when $\Delta\mu/kT \to -\infty$. No further increase in etching rate can be achieved at each temperature. We also found that orientations close to the thermodynamically stable (100) surfaces exhibit lower etching rates, with the (100) surface being the most resistant in etching. On the other hand, stepped surfaces exhibit larger etching rates than the (100) surface.

The role of surface diffusion on faceting and roughening transition in etching ($\Delta\mu < 0$) is demonstrated in Figs. 7(b) and 9(b). We have chosen a value of undersaturation where the interface does not exhibit distinct faceting ($-\Delta\mu/kT = 1$) in the absence of surface diffusion, as shown in Fig. 9(a). As the surface diffusion rises, local equilibrium is established at the interface, and faceting is observed under conditions where a kinetically rough interface would be expected and surface roughness decreases [Fig. 7(b)]. Increasing the surface diffusion coefficient results in a kinetically rough-to-faceted surface transition. Thus surface diffusion expands the window of operation conditions under which regular faceting is observed. The higher the surface diffusion the smaller the critical pressure below which the surface is faceted.

We have found that at sufficiently low temperatures ($kT/w_1 \leq 0.067$), where no faceting is observed under equilibrium conditions, surfaces can become faceted under etching conditions. That is, faceting can occur at lower temperatures under etching than under equilibrium conditions.

Figure 8(b) shows the effect of faceting on etching rate under conditions close to equilibrium. Faceting results in a slowing down of the etching rate. As time evolves, the etching rate approaches the etching rate of the (100) surface, which exhibits the lowest rate among all planes in the [010] zone.

VIII. COMPARISON OF GROWTH AND ETCHING MODES

The above analysis indicates that nonequilibrium conditions promote faceting because faceting occurs either at

lower temperatures than in equilibrium conditions or during shorter time, i.e., larger facets form under growth and etching conditions. On the other hand, kinetic roughening occurs at far from equilibrium growth and etching conditions, as shown in Figs. 6 and 9.

Deposition from the gas occurs at random positions, and if the supersaturation is sufficiently high rough interfaces rather than facets form. However, desorption of atoms is a local-environment-dependent process, as shown by Eq. (5). Single atoms on terraces have larger probability for desorption than atoms with more first-nearest neighbors. It is therefore important to examine more extensively the reversibility of the surface mode, i.e., whether rates and structures obtained during etching and deposition are alike. We have found that the growth and etching rates are not equal for the same absolute value of $\Delta\mu$ for growth from the gas phase; etching proceeds slower than growth at the same temperature.

To quantify the pictorial representation of promoted faceting under nonequilibrium conditions, we plot in Fig. 10(a) the probability density function $p(L/a_0)$ versus
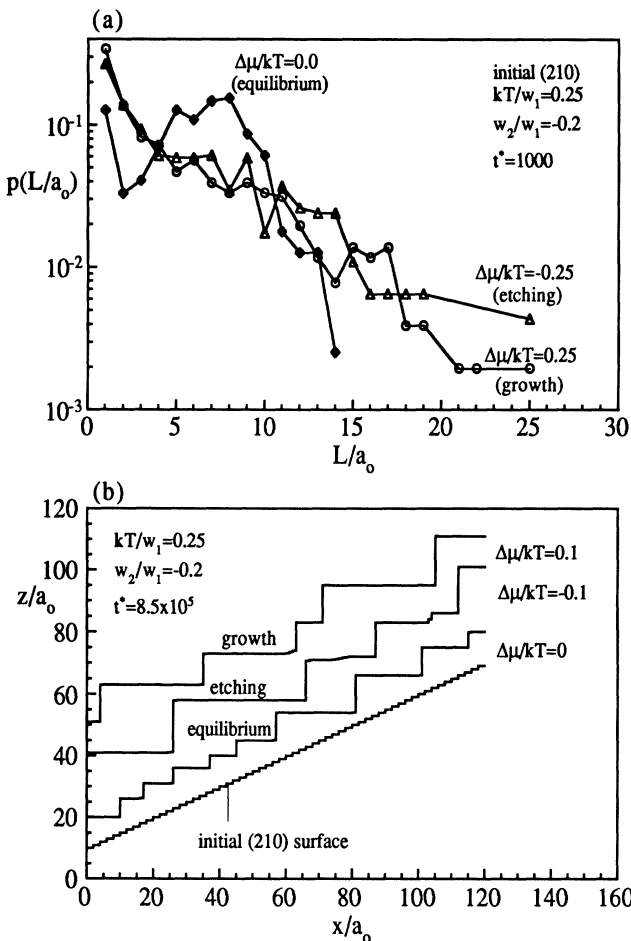

(a)

(b)

facet size L/a_0 calculated under equilibrium, growth, and etching conditions. After the same time, the largest facets developed in growth and etching are larger than the largest facets developed in equilibrium conditions. On the other hand, regions of the surface connecting facets are more rough in irreversible conditions, i.e., the probability density of small facets is larger in nonequilibrium conditions than in equilibrium conditions, especially for growth. Surface profiles after long time shown in Fig. 10(b) confirm that facets grow faster under irreversible conditions than under equilibrium conditions. That is, growth and etching promote faceting, especially at long times.

Simulations show that faceting can occur under nonequilibrium conditions at low temperatures where faceting is not observed under equilibrium conditions. Comparison of the time scales for faceting for both nonequilibrium modes reveals that faceting occurs much faster in growth than in etching. For example, at $kT/w_1 = 0.08$ the time required to attain $L/a_0 = 5$ is $t^* = 0.2$ for growth $(\Delta\mu/kT = 6)$ and $t^* = 1.4 \times 10^5$ for etching $(\Delta\mu/kT = -6)$ with $w_2/w_1 = -0.2$, i.e., difference by a factor of 10^6. The large perturbation (fluctuations) introduced by growth results in faster faceting compared to etching conditions. In that context, growth is a more efficient nonequilibrium mode for faceting than etching (metal evaporation).

The surface becomes kinetically rough under etching conditions if etching is very fast, but the surface is more resistant to kinetic roughening in etching than in growth. Figures 6(b), 7(b), and 9(b) indicate that a lower value of x_s/a_0 is required in etching than in growth for the transition from kinetically rough to faceted surfaces. Thus growth and etching from the gas phase are not reversible processes regarding surface morphology and especially in kinetic roughening.

We have also investigated the surface morphology under totally irreversible conditions at low temperatures where only desorption of material takes place without deposition $(\Delta\mu \rightarrow -\infty)$. It is found that at very low temperatures etching proceeds very slowly but faceting is still observed and thus, in contrast to growth, pure etching (without adsorption) results at the same temperature in faceted surfaces but not in kinetically rough surfaces, as happens if $\Delta\mu \gg 0$. In other words, surfaces are more resistant in kinetic roughening in etching than in deposition, and a larger parameter space is available for faceting in the bifurcation diagram.

IX. CONCLUSIONS

We have examined the faceting of unstable orientations with the MC method using adsorption-desorption and/or surface diffusion under equilibrium, growth, and etching conditions for simple cubic crystals. The main conclusions from these computer experiments can be summarized as follows:

(1) Quite regular distributions of facets are formed on surfaces, in agreement with experimental results.

(2) The facet size increases with time, indicating three fairly distinct time regimes: (a) disordering of surface

FIG. 10. Panel (a) shows the probability density of facet size distribution at $t^* = 1000$. Longer facets develop under nonequilibrium conditions. Panel (b) compares faceted surfaces under equilibrium, growth, and etching conditions at long times. Growth and etching promote faceting, especially at long times.

atoms where surface energy and surface roughening increase, (b) microfacet nucleation where small facets form, and (c) coarsening of microfacets into macrofacets by thermal fluctuations.

(3) At low temperatures faceting is limited by the transfer of material over long distances and faceting proceeds very slowly. At high temperatures thermal roughening rather than faceting occurs.

(4) Unstable interfaces which are very close to energetically stable interfaces either do not facet or facet very slowly. The most unstable orientations in the Wulff diagram facet first.

(5) Surface diffusion results in faceting in shorter times for small facets than adsorption-desorption.

(6) Transfer of material over long distances becomes important for small misorientations, at low temperatures, and/or long times (large facets). Adsorption-desorption alone is then more effective than migration in transport of material.

(7) Slight deviations from equilibrium conditions $(\Delta\mu\neq0)$ promote faceting and large deviations result in kinetic roughening.

(8) Growth promotes faceting more effectively than etching, especially at low temperatures.

(9) Simultaneous growth or etching and fast surface diffusion lead to promoted faceting and transition from rough to faceted surfaces. Surface diffusion results in faceted interfaces for conditions even far from equilibrium.

(10) The thermodynamically more unstable orientations become kinetically rough more easily in growth or etching. Thermodynamically stable surfaces are also more stable with respect to faceting or roughening and are the ones that would be observed under equilibrium, growth, or etching conditions.

The above model with first- and second-nearest-neighbor interactions is a simple one for simple cubic crystals. The simulations can be extended for metals by using a more realistic potential, such as the embedded atom, and for binary systems, such as alloys and compound semiconductors. However, we anticipate that the qualitative conclusions will not be altered appreciably. Research on these topics is in progress. The above model shows that the scaling law developed by Mullins, Eq. (2), is not valid, and faceting does not have as prerequisite irreversible conditions as previously has been suggested, i.e., thermodynamics alone can explain faceting. However, the thermodynamic instability can be enhanced under irreversible growth and etching conditions with simultaneous fast surface diffusion.

ACKNOWLEDGMENTS

*Author to whom correspondence should be addressed.

[1]M. Flytzani-Stephanopoulos and L. D. Schmidt, Prog. Surf. Sci. **9**, 83 (1979).

[2]C. Herring, in *Structure and Properties of Solid Surfaces* (Chicago University Press, Chicago, 1953), p. 5; Surf. Sci. **2**, 320 (1964).

[3]M. Wortis, in *Chemistry and Physics of Solid Surfaces VII*, edited by R. Vanselow and R. Howe (Springer-Verlag, New York, 1988), p. 367; Phys. Rep. **103**, 59 (1984).

[4]E. D. Williams and N. C. Bartelt, Ultramicroscopy **31**, 36 (1989); Science **251**, 393 (1991).

[5]G. Wulff, Z. Krist. **34**, 449 (1901).

[6]A. J. W. Moore, Acta Metall. **6**, 293 (1958); **8**, 646 (1960).

[7]A. J. W. Moore, in *Metal Surfaces* (American Society for Metals, Metals Park, OH, 1962), p. 155.

[8]R. Caracciolo and L. D. Schmidt, J. Electrochem. Soc. **130**, 603 (1983); A. J. Avria, J. C. Canullo, E. Custidiano, C. L. Perdriel, and W. E. Triaca, Electrochim. Acta **31**, 1359 (1986).

[9]M. G. Lagally, R. Kariotis, B. S. Swartzentruber, and Y. W. Mo, Ultramicroscopy **31**, 87 (1989).

[10]M. Asscher, J. Carrazza, M. M. Khan, K. B. Lewis, and G. A. Somorjai, J. Catal. **98**, 277 (1986); R. I. Masel, Catal. Rev. **28**, 335 (1986).

[11]R. Imbihl, A. E. Reynolds, and D. Kaletta, Phys. Rev. Lett. **67**, 275 (1991); J. Falta, R. Imbihl, and M. Henzler, Phys. Rev. Lett. **64**, 1409 (1990).

[12]W. W. Mullins, in *Metal Surfaces* (Ref. 7), p. 17.

[13]T. Engel, in *Chemistry and Physics of Solid Surfaces VII* (Ref. 3), p. 407; J. C. Heyraud and J. J. Metois, J. Cryst. Growth **82**, 269 (1987).

[14]N. Garcia, J. J. Saenz, and N. Cabrera, J. Phys. B **124**, 251 (1984).

[15]C. Herring, Phys. Rev. **82**, 87 (1951).

[16]W. W. Mullins and R. F. Sekerka, J. Phys. Chem. Solids **23**, 801 (1962).

[17]H. J. Leamy, G. H. Gilmer, and K. A. Jackson, in *Surface Physics of Materials I* (Academic, New York, 1975), p. 121.

[18]C. Rottman and M. Wortis, Phys. Rev. B **24**, 6274 (1981).

[19]J. E. Avron, H. van Beijeren, L. S. Schulman, and R. K. P. Zia, J. Phys. A **15**, L81 (1982).

[20]C. Rottman and M. Wortis, Phys. Rev. B **29**, 328 (1984).

[21]C. Jayaprakash and W. F. Saam, Phys. Rev. B **30**, 3916 (1984).

[22]A.-C. Shi and M. Wortis, Phys. Rev. B **37**, 7793 (1988).

[23]W. W. Mullins, Philos. Mag. **6**, 1313 (1961).

[24]W. W. Mullins, J. Appl. Phys. **28**, 333 (1957).

[25]H. P. Bonzel, E. Preuss, and B. Steffen, Appl. Phys. A **35**, 1 (1984).

[26]V. T. Binh, Y. Moulin, R. Uzan, and M. Drechsler, Surf. Sci. **79**, 133 (1979).

[27]G. Frohberg and P. Adam, Thin Solid Films **25**, 525 (1975); Acta Metall. **23**, 365 (1975).

[28]N. Cabrera, *Stability of the Structure of Crystal Surfaces,* Symposium on Properties of Surfaces (American Society for Testing and Materials, Philadelphia, 1962), p. 24; J. W. Cahn and J. E. Hilliard, J. Chem. Phys. **28**, 258 (1958); J. W. Cahn, Acta Metall. **9**, 795 (1961).

[29]M. S. Daw and M. I. Baskes, Phys. Rev. B **29**, 6443 (1989).

[30]J. F. Nicholas, Aust. J. Phys. **21**, 21 (1968).

[31]A. E. Blum and A. C. Lasaga, in *Aquatic Surface Chemistry,* edited by W. Stumm (Wiley, New York, 1987), p. 255.

[32]T. L. Hill, *An Introduction to Statistical Thermodynamics*

(Dover, New York, 1986).

[33]G. H. Gilmer, Science **25**, 208 (1980).

[34]N. Metropolis, A. W. Rosenbluth, M. N. Rosenbluth, A. H. Teller, and E. Teller, J. Chem. Phys. **21**, 1087 (1953).

[35]K. Kawasaki, Phys. Rev. **145**, 224 (1966); **148**, 375 (1966); **150**, 285 (1966).

[36]G. H. Gilmer and P. Bennema, J. Appl. Phys. **43**, 1347 (1972).

[37]D. G. Vlachos, L. D. Schmidt, and R. Aris, Surf. Sci. **249**, 248 (1991).

[38]W. K. Burton, N. Cabrera, and F. C. Frank, Philos. Trans. R. Soc. London Ser. A **243**, 299 (1951).

[39]A. B. Bortz, M. H. Kalos, and J. L. Lebowitz, J. Comput. Phys. **17**, 10 (1975).

[40]H. J. Leamy and G. H. Gilmer, J. Cryst. Growth **24/25**, 499 (1974).

[41]D. G. Vlachos, L. D. Schmidt, and R. Aris (unpublished).

[42]B. A. Cowans, K. A. Jurman, W. N. Delgass, Y. Z. Li, R. Reifenberger, and T. A. Koch, J. Catal. **125**, 501 (1990).

[43]D. R. Anderson, J. Catal. **113**, 475 (1988).

[44]S. Balibar, F. Gallet, and E. Rolley, J. Cryst. Growth **99**, 46 (1990), and references therein.

[45]M. Elwenspoek and J. P. van der Eerden, J. Phys. A **20**, 669 (1987).

[46]R.-F. Xiao, J. I. D. Alexander, and F. Rosenberger, J. Cryst. Growth **100**, 313 (1990), and references therein.

[47]P. Nozieres and F. Gallet, J. Phys. (Paris) **48**, 353 (1987).